Nuclear Instruments and Methods in Physics Research A 626–627 (2011) 114–119

Contents lists available at ScienceDirect

Nuclear Instruments and Methods in Physics Research A

journal homepage: www.elsevier.com/locate/nima

A Compton imager for in-vivo dosimetry of proton beams—A design study

T. Kormoll [a,*], F. Fiedler [b], S. Schöne [b], J. Wüstemann [a], K. Zuber [c], W. Enghardt [a,b]

[a] Technische Universität Dresden, OncoRay—Center for Radiation Research in Oncology, Fetscherstr. 74, 01307 Dresden, Germany
[b] Forschungszentrum Dresden-Rossendorf, Institute for Radiation Research, Bautzner Landstr. 400, 01328 Dresden, Germany
[c] Technische Universität Dresden, Institute for Nuclear and Particle Physics, Zellescher Weg 19, 01069 Dresden, Germany

ARTICLE INFO

Article history:
Received 24 August 2010
Received in revised form
8 October 2010
Accepted 8 October 2010
Available online 5 November 2010

Keywords:
Compton imaging
Dosimetry
Single photon emission computed tomography
Simulation
Semiconductor detectors
Proton and ion radiotherapy

ABSTRACT

In-beam SPECT during therapeutic proton beam irradiation is a novel method for three dimensional in-vivo dose verification. For this purpose a Compton camera design is evaluated with respect to the special requirements and conditions that arise from this application. Different concepts are studied by means of simulation concerning the angular resolution and efficiency. It was found that a cadmium zinc telluride system can perform sufficiently well. For further evaluation the construction of a semiconductor scintillator hybrid system is under way.

1. Introduction

In-vivo dose monitoring during tumor irradiation can improve the therapy by verifying the dose distribution in and around the target volume. This holds true especially for ion beam treatment since the dose profile is very sensitive to anatomical changes or minor positioning uncertainties. One of the methods for dose verification is in-beam positron emission tomography (PET), which relies on the production of positron emitters—predominantly ^{11}C and ^{15}O from projectile and target fragmentation. However, because of geometrical restriction a conventional ring PET scanner cannot be installed at the irradiation facility. Only a double head positron camera is possible, which suffers from limited angle artifacts [1]. This limitation can be circumvented by off-beam PET, i.e. moving the patient to a conventional PET scanner after treatment [2]. But in this method the radioactive nuclides are subject to metabolic processes, e.g. blood flow, and thereby the image quality and in particular the relationship between dose and activity is degraded.

In-beam single photon emission computed tomography (SPECT) can be a method more feasible for ion treatment. Since in-beam SPECT registers prompt γ-rays following nuclear reactions between projectiles and atomic nuclei of tissue, it is not influenced by metabolism. Since no detectors opposite to each other are required less artifacts because of restricted camera geometries are expected. Conventional SPECT however is not feasible because the emission spectrum is highly energetic and would require impractically thick collimators. Hence, a Compton camera approach is pursued. It has been shown by others that in-vivo dosimetry by means of Compton imaging may be possible [3].

In this work angular resolution and efficiency of a Compton camera with respect to the special conditions and requirements of in-beam SPECT are studied. Based on the result the concept of an evaluation system is presented, which is currently under construction.

2. Materials and methods

The long-term aim is to design a system that operates under clinical conditions. A spatial resolution of the order of a few millimeters is required for extracting distribution parameters with a precision of 1–2 mm from the images. For beam localization in three dimensions a design with several heads facing the patient from different directions is under consideration. Each head is a single Compton camera comprising several detector layers. The minimum possible distance from the camera heads to the beam is assumed to be 25 cm. The emission spectrum of a water phantom irradiated with 200 MeV protons was acquired from a Monte Carlo simulation (Fig. 1). Details are presented in Ref. [4]. The emission spectrum is in the range of MeV and is dominated by a number of discrete γ-lines from nuclear de-excitations. The most prominent lines are 511 keV (positron annihilation), 2.2 MeV (deuterium), 4.4 MeV (carbon) and 6.1 MeV (oxygen). An imaging system should

* Corresponding author.
E-mail address: thomas.kormoll@physik.tu-dresden.de (T. Kormoll).

0168-9002/$ - see front matter © 2010 Elsevier B.V. All rights reserved.
doi:10.1016/j.nima.2010.10.031

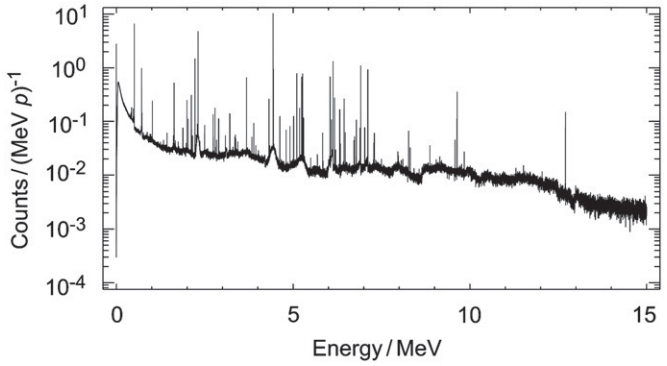

Fig. 1 Photon emission spectrum of a water phantom irradiated with 200 MeV protons [4].

be able to resolve these lines in order to estimate the carbon-to-oxygen ratio, which can be a measure for the tissue type.

The fluence rate at the detector position is in the order of 10^3 photons cm^{-2} s^{-1} for an irradiation time of 300 s and a delivered dose of approximately 1 Gy. In in-beam PET imaging, a good image is made of 150 000 events. Assuming that this value holds for Compton imaging as well, a Compton camera of an area of 12×12 cm^2 and an efficiency of 0.3% is needed. A larger camera with lower efficiency is also feasible. However, the number of signal processing channels will scale with detector size. Moreover, the coincidence rate compared to single events is lower in a camera with low efficiency. Therefore, it is desirable to have high efficiency, which allows for a small camera in order to simplify the logic and to increase the signal-to-noise ratio.

Two detection principles are under consideration. Both rely on the reconstruction of cones whose surface denotes the possible origin of the photon. For conventional Compton imaging an incoherent scatter event followed by complete absorption is required. The scattering angle φ can be calculated from the energy depositions L_1 and L_2 in the scatter and absorption detector, respectively:

$$\cos\varphi = 1 - mc^2\left(\frac{1}{L_2} - \frac{1}{L_1+L_2}\right) \tag{1}$$

where m is the electron rest mass and c the speed of light. Measured quantities are the two energy depositions for the calculation of the opening angle and the two interaction positions for determining the cone axis.

There is another technique that requires two subsequent scatterings and a third interaction of any kind [5]. Measured quantities are the energy depositions at the two scatter sites L_1 and L_2, their position and the position of the last interaction. The opening angle of the cone can be calculated using the energy depositions and the second scattering angle φ_2, which can be deduced from the three position measurements:

$$\cos\varphi = 1 - mc^2\left(\frac{1}{E_0(L_1,L_2,\varphi_2)-L_1} - \frac{1}{E_0(L_1,L_2,\varphi_2)}\right)$$
$$E_0(L_1,L_2,\varphi_2) = L_1 + \frac{L_2}{2} + \frac{1}{2}\sqrt{L_2^2 + \frac{4mc^2L_2}{1-\cos\varphi_2}} \tag{2}$$

E_0 is the incident energy of the photon. Since there is no need for full absorption it is not simply the sum of the deposited energies. The absorption probability limits the overall efficiency of a conventional Compton camera. Therefore, better efficiency at high photon energy is expected from this technique.

The detector materials high purity germanium (HPGe) and CdZnTe (CZT) have been examined. This work is focused on semiconductors because of the depth of interaction capability and better spatial resolution compared to scintillators.

2.1. Angular resolution

The resolution of a Compton imager is affected by energy resolution, spatial resolution and Doppler broadening. The energy resolution and the Doppler broadening influence the calculated cone angle only; the spatial resolution is important for the cone axis and in the twofold scattering technique for the determination of the second scattering angle, which in turn influences the calculated opening angle.

2.1.1. Energy resolution

The influence of energy resolution on angular resolution has been studied applying error propagation to Eqs. (1) and (2) with respect to all measured quantities under the condition that the incident energy is unknown. Covariance terms have been neglected in both cases.

From Eq. (1), the uncertainty in φ can be written as

$$(d\varphi)^2 = T_1^2\left(\frac{dL_1}{L_1}\right)^2 + T_2^2\left(\frac{dL_2}{L_2}\right)^2; T_1 = \frac{mc^2L_1}{(L_1+L_2)^2\sin\varphi},$$
$$T_2 = \frac{mc^2L_2^2}{\sin\varphi}\left(\frac{1}{L_2^2} - \frac{1}{(L_1+L_2)^2}\right) \tag{3}$$

Formula (2) gives:

$$(d\varphi)^2 = T_1^2\left(\frac{dL_1}{L_1}\right)^2 + T_2^2\left(\frac{dL_2}{L_2}\right)^2 + T_3^2(d\varphi_2)^2; T_1 = \frac{mc^2L_1}{E_0^2\sin\varphi},$$
$$T_2 = \frac{mc^2L_2}{\sin\varphi}\left(\frac{1}{(E_0-L_1)^2} - \frac{1}{E_0^2}\right)\left(\frac{1}{2} + \frac{1}{4}\sqrt{L_2^2+XL_2^{-1}}(2L_2+X)\right),$$
$$T_3 = \frac{\sin\varphi_2 mc^2}{4\sin\varphi}\left(\frac{1}{(E_0-L_1)^2} - \frac{1}{E_0^2}\right)\sqrt{L_2^2+XL_2^{-1}}\left(\frac{XL_2}{1-\cos\varphi_2}\right),$$
$$X = 4mc^2/(1-\cos\varphi_2) \tag{4}$$

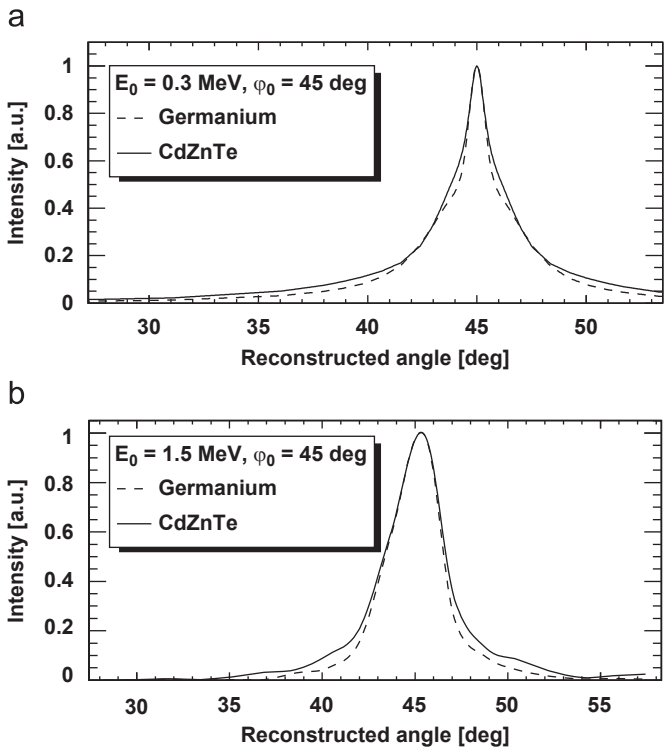

Fig. 2. (a) Distribution of events according to the reconstructed scattering angle due to Doppler broadening in the scatter–absorber technique. (b) Distribution of events according to the reconstructed scattering angle due to Doppler broadening in the scatter–scatter technique.

All terms resulting from uncertainties in energy measurement decrease with increase in photon energy. In order to get functions $\Delta\varphi(E_0,\varphi)$, i.e. the angular uncertainty in dependence of the scattering angle on incident energy, a model for energy resolution is needed. The following models have been used:

$$\text{germanium}: \Delta E = 2\,\text{keV}$$

$$\text{CZT}: \Delta E = 6\,\text{keV} + 0.15\,\text{keV}\sqrt{E/\text{keV}} \quad (5)$$

The value for germanium is motivated from Ref. [6]. The CZT model is a plausible assumption based on energy resolution values given in Ref. [7].

2.1.2. Doppler broadening

The contribution from Doppler broadening has been accounted for using the differential cross-section for scattering off a bound electron [8] and the Compton profiles [9], i.e. the impulse approximation model of incoherent scattering has been used. In the case of the scatter–absorber technique at a given incident energy and at a given scatter angle the cross-sections for scattering into all possible energies have been calculated. Subsequently for each energy of the scattered photon the angle according to Eq. (1) has been calculated based on the deposited energy in the scattering event and the remaining energy. Each angle corresponds to a value of the Ribberfors cross-section of Ref. [8] so that the cross-section has been transformed into an angular distribution. Examples of these distributions are given in Fig. 2a. They are centered around the angle that was entered into the calculation. The broad tail is due to the core electrons, which have large momentum. The sharp peak comes from the loosely bound valence electrons. As a measure of width the full width at half maximum (FWHM) has been used.

In the case of the twofold scattering technique a simple Monte Carlo approach has been used for obtaining the angular distribution. First, the energy after the first event has been randomly selected following the cross-section. Second, this step has been repeated for the second event. The second scattering angle has been kept fixed like in the first event. Now the first scattering angle has been calculated according to deposited energies and the second scattering angle. This has been done several times and all reconstructed angles were entered into a histogram, which forms the angular distribution. An example of such a distribution for the scatter–scatter technique is given in Fig. 2b. The FWHM has been determined by fitting a pseudo-Voigt function and calculating its FWHM.

2.1.3. Geometrical effects

The pixel size is assumed to be 1 mm × 1 mm and the depth of interaction accuracy to be 0.5 mm. The angular accuracy of the cone

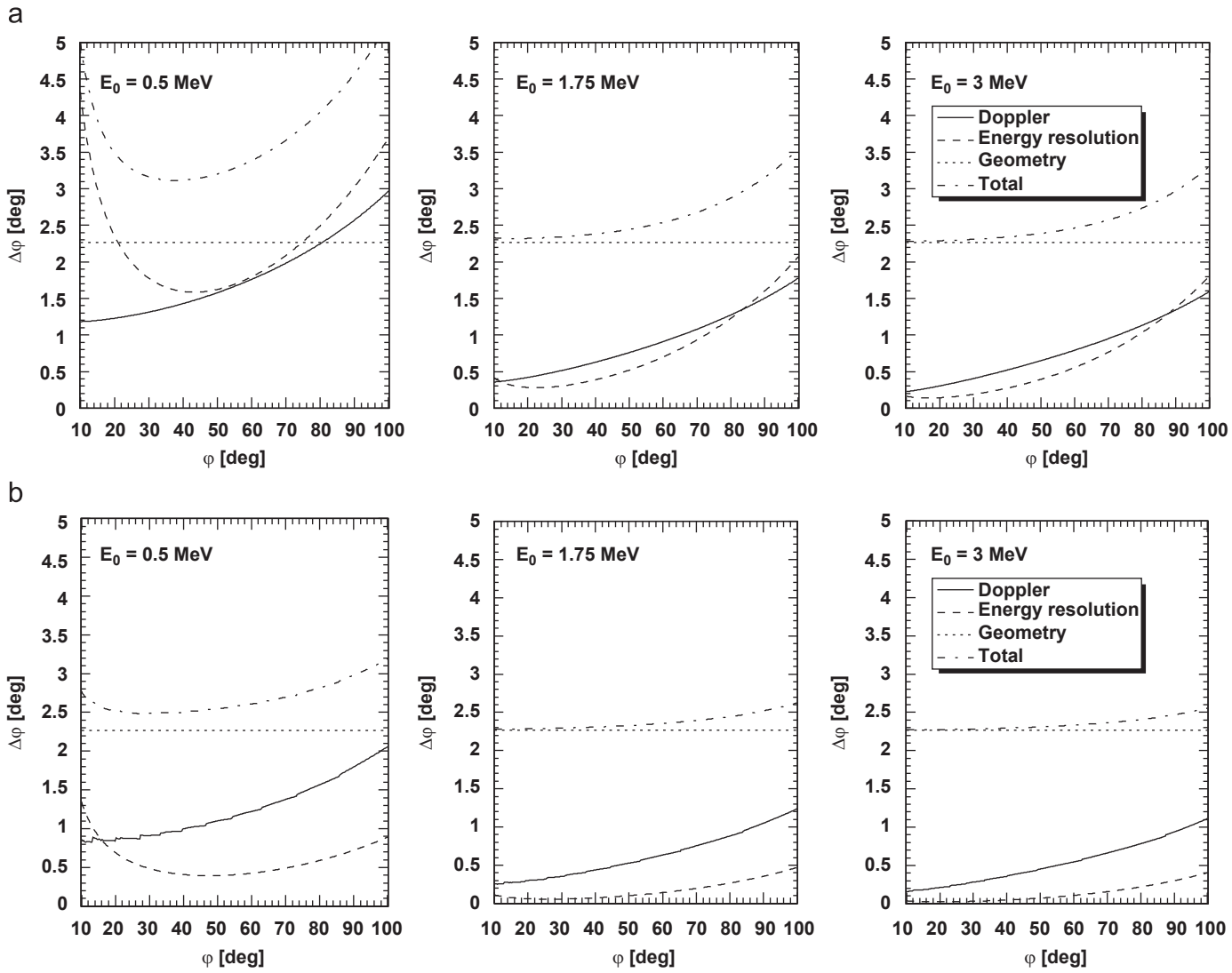

Fig. 3. (a) Angular uncertainties of a CdZnTe system in scatter–absorber configuration. (b) Angular uncertainties of a Ge system in scatter–absorber configuration.

axis not only depends on the scattering angle but also on the entrance angle. To reduce the number of degrees of freedom in the following analysis the geometrical errors were assumed to be maximal. In the case of the scatter–scatter method the accuracy of the second scattering angle was assumed to be 2°. This roughly corresponds to a detector with a pixel size of 1 mm × 1 mm at a distance of 4 cm.

2.2. Efficiency

Efficiency heavily depends on the energy of the incident photon. Especially for valid events in the simple Compton technique the required absorption limits the efficiency.

To evaluate this and the dependence on geometrical parameters a custom simplified Monte Carlo program has been developed, which tracks photons through a simple geometry of several detector layers. For this purpose cross-sections from the XCOM database have been used [10]. In the event of incoherent scattering the Klein–Nishina expression for the differential cross-section was applied [11]. The only interactions that can occur within this program are photoelectric absorption, incoherent scattering and pair production in the nuclear Coulomb field. If an event other than incoherent scattering occurs the tracking of this special photon is aborted since this photon either cannot yield a valid event any longer in the sense of cone reconstruction or already has a history of a good event. Particles other than photons are not tracked. Due to these simplifications this Monte Carlo code is not suitable for the generation of event data, but it is capable of deciding whether a photon history leads to a valid event or not. This code runs faster than a full Monte Carlo simulation with Geant4 for example and because of its simple structure there is less danger of missing a crucial item when tuning a fully featured code to simplified interactions.

The calculated efficiency is the number of photons that have a history that gives a valid event, i.e. either incoherent scattering followed by photoelectric absorption or two subsequent scatterings followed by a third interaction in a different layer, divided by the total number of incident photons in the detector setup.

3. Results

3.1. Angular resolution

The angular resolutions in the scatter–absorber method with different materials as scatter and absorber detectors are presented

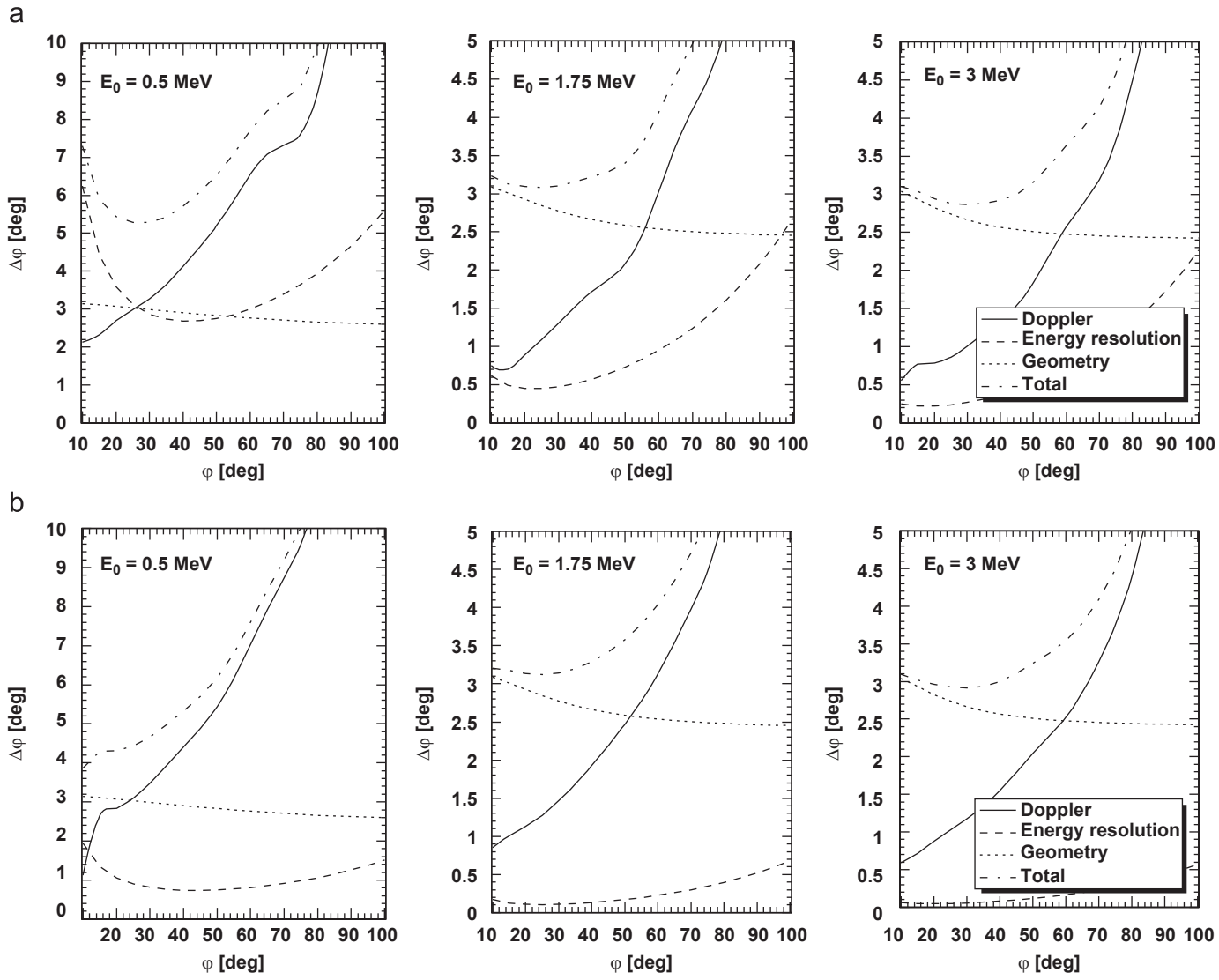

Fig. 4. (a) Angular uncertainties of a CdZnTe system in scatter–scatter configuration. (b) Angular uncertainties of a Ge system in scatter–scatter configuration.

in Fig. 3a and b. They are calculated for three different incident energies and are plotted as dependence on the scattering angle. In general the angular resolution is dominated by energy resolution and Doppler broadening in the low energy regime while it becomes geometry dominated at high energies.

The results from the scatter–scatter technique are shown in Fig. 4a and b for a stack of germanium and CdZnTe detectors. Here, the second scattering angle has been kept fixed to reduce the number of degrees of freedom. It has been found by variation of the second angle that it does not heavily influence the overall resolution. The trend is the same as in the scatter–absorber method. The higher the energy the less important the material properties. Especially the Doppler part is not so different for germanium and CdZnTe. This is in good agreement with the work of Zoglauer and Kanbach [12]. The total resolution is slightly worse than in the simpler technique because of the additional contribution from the second angle measurement.

3.2. Efficiency

In Fig. 5 the efficiency of a system of three and five layers is shown. The left two graphics display the efficiency of a germanium system; CdZnTe is shown on the right. The upper row plots are the efficiency for the scatter–absorber technique; in the lower row the scatter–scatter efficiency is presented. Two different layer thicknesses were studied—5 and 10 mm. All systems have an area of 12×12 cm^2.

The more the layers of the system, the higher the efficiency. The five-layer systems have approximately twice the efficiency as that of the three-layer systems. It can also be seen that thicker layers yield better efficiency. The CdZnTe detectors have nearly identical efficiency in the scatter–scatter regime but a better scatter–absorber efficiency compared to germanium.

4. Discussion and conclusion

The concept of a Compton camera consisting of semiconductor layers for in-vivo dosimetry has been investigated in terms of angular resolution and efficiency. The considerations presented in this study are not complete. Effects like cross talk due to large charge clouds at high energy depositions, see e.g. Ref. [13], and random coincidences have not been considered, yet. Nevertheless, there are indications that a CdZnTe system can perform nearly as well as a germanium system in the MeV energy range. The efficiency is even better due to the higher atomic number.

The performance with all effects under clinical conditions needs to be further studied. For this purpose a small evaluation system is under construction. This system will be composed of two CdZnTe layers of the size 20 mm $\times$ 20 mm $\times$ 5 mm and one LSO scintillator block with a modified Anger light readout. The LSO block will be 52 mm $\times$ 52 mm $\times$ 20 mm in size. With this layer, the scatter–absorber efficiency will be raised to approximately 0.7% at 1 MeV. Thereby it is possible to use this system for real imaging despite its small size. On the other hand it will give an opportunity to study scatter–scatter events since it consists of three layers.

The CdZnTe detectors will be configured as cross strip detectors with 16+16 strips to make the discrete electronics concept feasible, which allows fast readout. This system is designed to study the CdZnTe performance, the logic of event selection and to explore different concepts of neutron shielding. In parallel, image

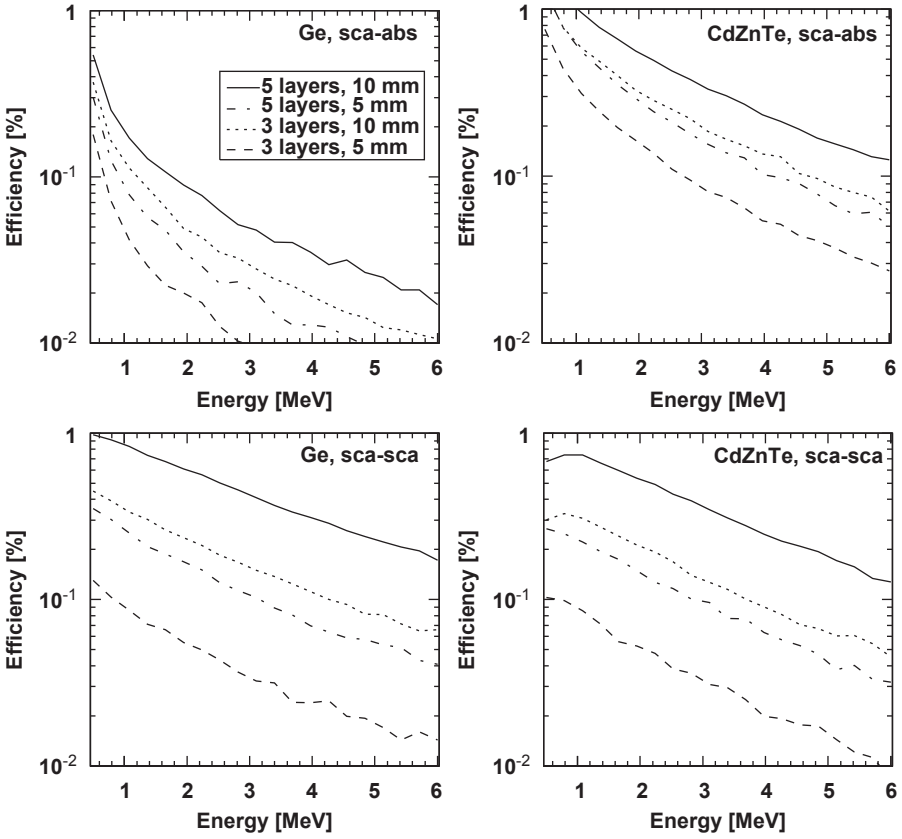

Fig. 5. Efficiency of germanium and CdZnTe systems with three and five layers in scatter–scatter (“sca–sca”) and scatter–absorber (“sca–abs”) techniques.

reconstruction algorithms are developed, which are meant to be tested with the evaluation system as well.

References

[1] G. Shakirin, H. Braess, F. Fiedler, D. Kunath, K. Laube, K. Parodi, M. Priegnitz, W. Enghardt, IEEE NSS/MIC Conference Record, 2009, p. 2792.
[2] K. Parodi, T. Bortfeld, W. Enghardt, F. Fiedler, A. Knopf, H. Paganetti, J. Pawelke, G. Shakirin, H. Shih, Nucl. Instr. and Meth. A 591 (2008) 282.
[3] S. Kabuki, K. Ueno, S. Kurosawa, S. Iwaki, H. Kubo, K. Miuchi, Y. Fujii, D. Kim, J. Kim, R. Kohara, O. Miyazaki, T. Sakae, T. Shirata, T. Takayanagi, T. Terunuma, Y. Tsukahara, E. Yamamoto, K. Yasuoka, T. Tanimori, IEEE NSS/MIC Conference Record, 2009, p. 2437.
[4] F. Fiedler, T. Kormoll, A. Müller, W. Enghardt, in: Proceedings of the IEEE NSS/MIC Conference, 2010, p. N40-1.
[5] J.D. Kurfess, W.N. Johnson, R.A. Kroeger, B.F. Phlips, AIP Conf. Proc. 510 (2000) 789.
[6] K. Vetter, M. Burks, C. Cork, M. Cunningham, D. Chivers, E. Hull, T. Krings, H. Manini, L. Mihailescu, K. Nelson, D. Protic, J. Valentine, D. Wright, Nucl. Instr. and Meth. A 579 (2007) 363.
[7] F. Zhang, Z. He, G.F. Knoll, D.K. Wehe, J.E. Berry, IEEE Trans. Nucl. Sci. NS52 (2005) 2009.
[8] R. Ribberfors, Phys. Rev. B 12 (1975) 2067.
[9] F. Biggs, L.B. Mendelsohn, J.B. Mann, At. Data Nucl. Data 16 (1975) 201.
[10] M.J. Berger, J.H. Hubbell, S.M. Seltzer, J. Chang, J.S. Coursey, R. Sukumar, D.S. Zucker, NIST Standard Reference Database, 〈http://www.nist.gov/pml/data/xcom/index.cfm〉, accessed 2010.
[11] O. Klein, Y. Nishina, Z. Phys. 52 (1929) 853.
[12] A. Zoglauer, G. Kanbach, Proc. SPIE 4851 (2003) (2003) 1302.
[13] F. Zhang, W.R. Kaye, Z. He, IEEE NSS/MIC Conference Record, 2009, p. 2012.